Trans Indian Inst Met (2018) 71(4):873–882
https://doi.org/10.1007/s12666-017-1219-2

TECHNICAL PAPER

Investigation of Microstructure, Mechanical and Wear Behaviour of B_4C Particulate Reinforced Magnesium Matrix Composites by Powder Metallurgy

Fatih Aydin[1] · Yavuz Sun[1] · Hayrettin Ahlatci[1] · Yunus Turen[1]

Received: 16 June 2017 / Accepted: 20 October 2017 / Published online: 28 October 2017

Abstract In the present study, magnesium and magnesium matrix composites reinforced with 10, 20 and 30 wt% B_4C particulates were fabricated by powder metallurgy using hot pressing technique. The microstructure, mechanical properties and wear behaviour of the samples were investigated. Microstructure characterization showed generally uniform distribution of B_4C particulates. XRD investigations revealed the presence of Mg, B_4C and MgO phases. The mechanical properties of the investigated samples were determined by hardness and compression tests. Hardness and compressive yield strength significantly increased with increasing B_4C content. The reciprocating wear tests was applied under loads of 5, 10 and 20 N. Wear volume losses decreased with increasing B_4C content. Abrasive and oxidative wear mechanisms were observed.

Keywords B_4C · Powder metallurgy · Hot pressing · Microstructure · Wear behaviour · Mechanical properties

1 Introduction

Magnesium (Mg) is the sixth most abundant element in the earth and has low density (1.738 g/cm^3) and high specific strength [1]. Hardness, specific strength, wear resistance, creep and fatigue properties of pure Mg significantly increase with the addition of reinforcement elements [2]. Therefore, magnesium metal matrix composites (Mg-MMCs) are one of the most investigated materials because of their improved strength, stiffness, abrasion and oxidation resistance [3]. Mg-MMCs are promising materials for automotive and aerospace industry applications due to their better mechanical and physical properties [4].

There are several production methods for Mg-MMCs. These are pressureless infiltration [5], powder metallurgy [6], stir casting and squeeze casting [7]. Powder metallurgy provides the distribution of homogeneous particulates and causes less reaction between matrix and reinforcement [8]. Therefore, powder metallurgy has been chosen as production method for this study.

SiC [9–11], Al_2O_3 [12, 13], TiC [14] and CNT [15] are the most common reinforcements which are used for MMCs. B_4C is a reinforcement material which has high melting point, thermal stability, extreme abrasion resistance, high hardness and low density [16]. There are several studies on Mg/B_4C composites by infiltration process [5, 17, 18]. Also, there are some studies on Mg/B_4C composites that include cold pressing followed by sintering which is known as conventional powder metallurgy [6, 19]. In one of those studies, Ghasali et al. [6] produced B_4C reinforced Mg-MMCs and investigated bending strength and hardness of the composites. Jiang et al. [19] also fabricated Mg/B_4C composites and studied wear behaviour. They didn't include enough configurations to obtain deeper information on wear mechanisms. However, no detailed study has been observed on microstructure, mechanical properties (compression strength), wear behaviour and wear mechanism on Mg/B_4C composites by powder metallurgy (using hot pressing technique) in the literature. Hot pressing enables to manufacture different materials which are difficult to produce by conventional powder metallurgy.

The purpose of this study is to investigate the producibility of Mg/B_4C composites with high weight fraction by powder metallurgy. At the same time, microstructure,

✉ Fatih Aydin
fatih.aydin@karabuk.edu.tr

[1] Metallurgy and Materials Engineering Department, Karabuk University, 78050 Karabuk, Turkey

Table 1 Chemical composition of Mg powder

Element	Mg	Al	Si	Mn	Fe	Ni	Cu
Wt%	99.869	0.037	0.068	0.013	0.007	0.004	0.002

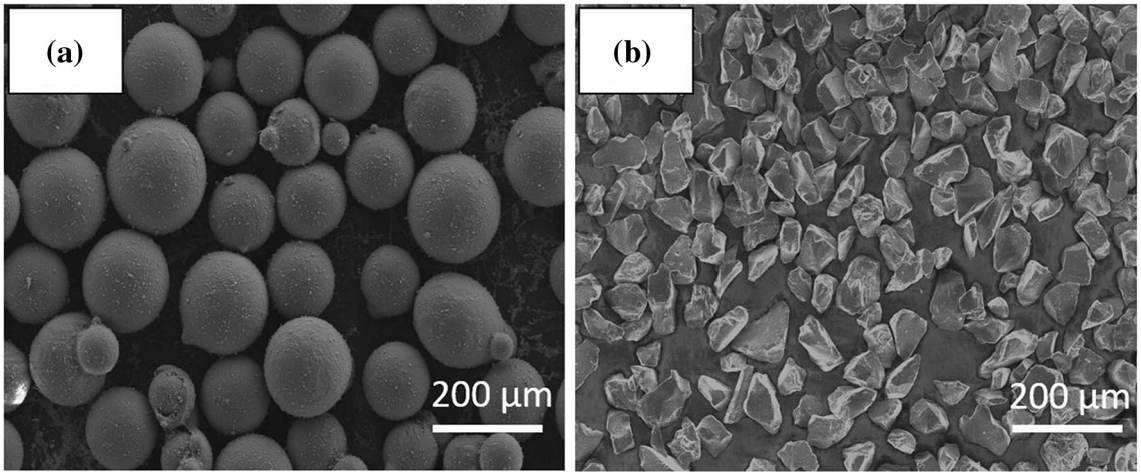

Fig. 1 SEM images of powders **a** pure Mg, and **b** B_4C

mechanical properties and wear behaviour of the specimens were investigated in detail. Firstly, pure Mg and MMCs were produced. Then, microstructure characterization was carried on with SEM, EDX and XRD. Hardness and compression tests were done on samples to determine mechanical properties. To examine wear behaviour, the reciprocating wear tests were applied under loads of 5, 10 and 20 N. The morphology of worn out surfaces was investigated using SEM to assess the mechanism of wear.

2 Experimental Procedure

In this study, magnesium (99.87% purity, ~ 110 µm) and B_4C powders (~ 40 µm) were used. Powders were supplied from Nanografi Company in Turkey. Chemical composition of Mg powder is given in Table 1.

Figure 1 shows the SEM images of Mg and B_4C powders used here. The average particle size of pure Mg powder was 103–129 µm and of B_4C powder was 35–53 µm. Figure 2 shows the XRD patterns of the Mg and B_4C powder. From the XRD results, it could be seen that Mg and B_4C phases were detected due to high purity of powders.

Pure Mg and MMCs containing 10, 20 and 30 wt% of B_4C particulates were manufactured by powder metallurgy using hot pressing. To obtain uniform particulate distribution, powders were mixed with turbulamixer for 4 h. Pure Mg and MMCs were produced at 600 °C under 50 MPa for 12 min in hot pressing machine (Material

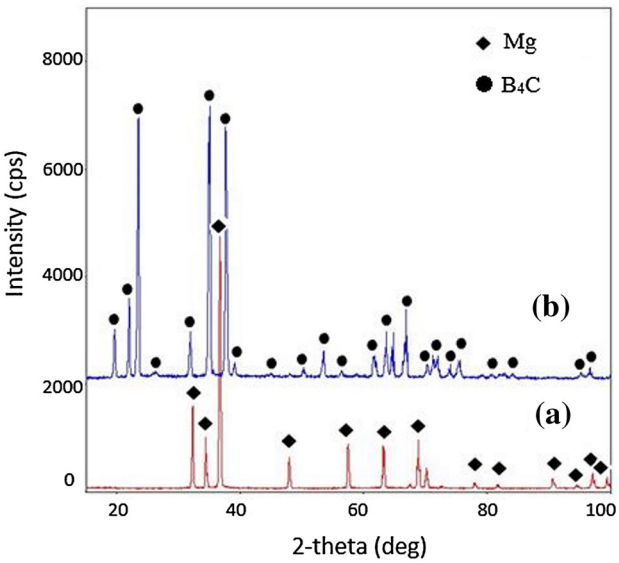

Fig. 2 XRD patterns of powders **a** pure Mg, and **b** B_4C

Science Engineering, MSE HP_1200). After pressing, sintering was done at 600 °C for 1.5 h. Argon was used as a protective atmosphere. Figure 3 shows the graphite die and produced samples. The dimensions of samples were about 15 mm (diameter) and 23 mm (height). Sintering parameters used in this study for production of pure Mg and MMCs are given in Table 2.

Theoretical densities of pure Mg and MMCs were calculated using the rule of mixture principle. Actual densities of specimens were performed using three successive

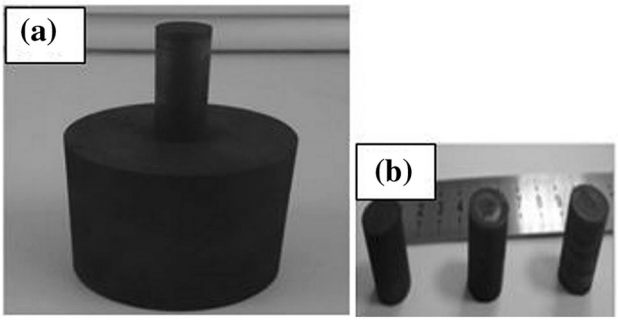

Fig. 3 Images of **a** graphite die, **b** produced samples

Table 2 Sintering parameters used in this study

Pressure	50 MPa
Pressure time	12 min
Pressure temperature	600 °C
Sintering time	90 min
Sintering temperature	600 °C
Atmosphere	Argon

measurements for each sample in accordance with Archimedes principle [20]. A Radwag electronic balance with 0.1 mg accuracy was used for measurement. Distilled water was used as fluid for measurements.

Microstructural characterization of the samples was done using scanning electron microscope (SEM, Carl Zeiss Ultra Plus) equipped with an energy dispersive spectrometer (EDS, Bruker X Flash 6/10). The phase identification was carried out using XRD machine (Rigaku Ultima IV) with Cu K_α radiation (λ: 1.54A°) at 2°/min scanning speed. Diffraction patterns were obtained with 2 theta (Bragg angle) between 15° and 100°.

Hardness values of the samples were determined using five successive indentations for each sample with hardness machine (Qness, Q10 A+) under a load of 0.5 kg for 15 s. Compression tests were applied in accordance with ASTM E9 standard using a Zwick/Roell 600kN test machine. The dimensions of compression test specimens were 15 mm (diameter) and 15 mm (height).

The reciprocating wear tests were conducted with a tribometer test device (UTS, T10/20) under loads of 5, 10 and 20 N. AISI 52100 steel was used as counter-face material. Wear test parameters are given in Table 3. After wear tests, wear volume was calculated using wear depth, wear width and stroke distance. Wear area was accepted as a parabola. Wear area was calculated using parabola area formula [21]. To calculate wear volume loss (mm^3/m), wear volume was divided by sliding distance.

Table 3 Wear test parameters

Load	5, 10 and 20 N
Stroke	8 mm
Counter-face material	AISI 52100 steel
Frequency	4 Hz
Sliding distance	500 m
Sliding speed	64 mm/s
Temperature and humidity	23 °C, 17%

3 Results and Discussion

3.1 Density Results

The theoretical density, actual density and porosity of pure Mg and MMCs are given in Table 4. As seen in Table 4, actual densities of the materials are lower than theoretical densities. It can be seen that the percentage of porosity increases with the addition of B_4C particulates. This can be attributed to the agglomeration of high content B_4C which leads to the formation of porosity in the structure [22]. The increase in porosity with increasing reinforcement content is completely consistent with the previous studies [23, 24]. It can be concluded that the difference between theoretical and actual density is related to the presence of fine micropores [23, 25]. The densities of produced composites are significantly affected due to shrinkage during sintering process. Also, the tremendous difference in melting point and compressive strength of powders has a significant effect on densities of the composites [26]. To get higher actual densities, different size of particulates, sintering times and sintering temperatures can be tried. However, this can be a topic of our future studies.

Researchers reported the presence of MgO in Mg-MMCs in literature [19, 27, 28]. Generally, the presence of MgO in the structure is attributed to high chemical activity between Mg and O during sintering. However, there is no clear explanation about the effect of MgO on sintered density in Mg-MMCs in these studies. Baghchesara et al. [29] also produced MgO reinforced Al matrix composites by powder metallurgy. They reported that the presence of MgO has negative effect on sinterability due to its high

Table 4 Theoretical, actual density and porosity of pure Mg and MMCs

Material	Theoretical density (g/cm^3)	Actual density (g/cm^3)	Porosity %
Pure Mg	1.738	1.712	1.495
Mg/wt% 10 B_4C	1.812	1.773	2.152
Mg/wt% 20 B_4C	1.891	1.847	2.326
Mg/wt% 30 B_4C	1.969	1.893	3.859

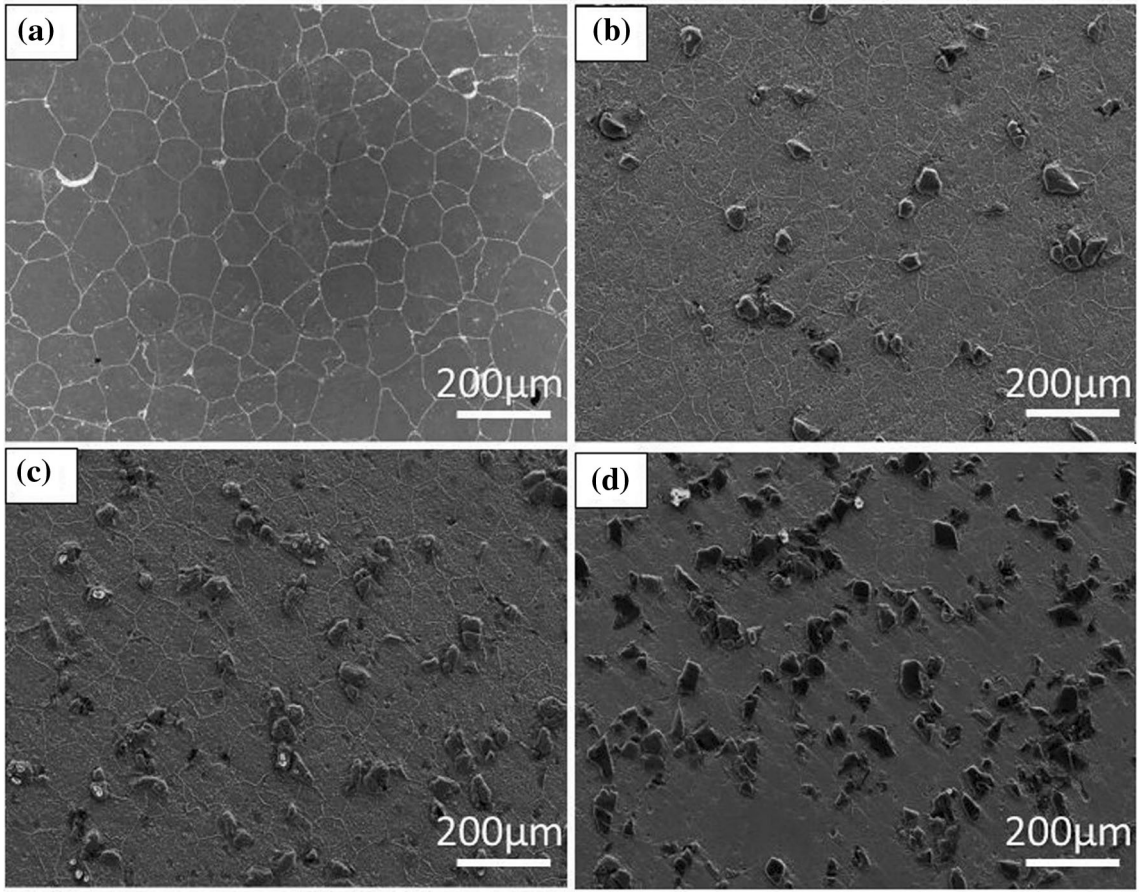

Fig. 4 SEM images of **a** pure Mg, **b** Mg/10 wt % B_4C, **c** Mg/20 wt % B_4C, **d** Mg/30 wt% B_4C

melting point (2780 °C). The negative effect of MgO on densification may be attributed to the adverse effect on specimens compaction during sintering. This leads to the formation of porosities which hinders achievement of higher actual densities. In this study, it is possible to say that the presence of the MgO has an adverse effect on sinterability of specimens which increases the porosity. Based on EDS results (Fig. 6), it can be seen that the content of MgO is too low. It is believed that this effect is negligible for this study.

3.2 Microstructure Characterization

Figure 4 shows the SEM images of pure Mg and MMCs. Grain boundaries are clearly observed in pure Mg. As seen in SEM images of MMCs, homogenous distribution of particulates are observed in all composites. Agglomeration of B_4C particulates is not observed in Mg/10 wt% B_4C and Mg/20 wt% B_4C. However, partial agglomeration in Mg/30 wt% B_4C is discernible (Fig. 5). Micro and macro porosities are not obviously seen in the microstructure because of low porosity content (Table 4). The average grain size of pure Mg is about 124 µm, while grain sizes of

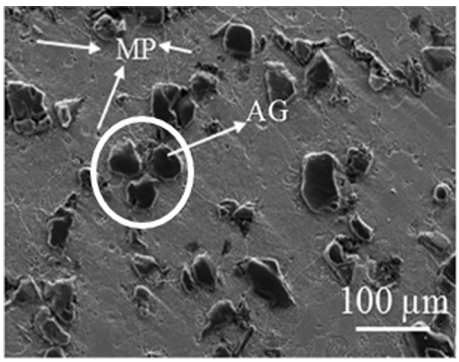

Fig. 5 SEM image of Mg/30 wt% B_4C composite

10, 20 and 30 wt% B_4C composites are measured as 99, 84 and 92 µm, respectively. Therefore, it can be said that grain coarsening is hindered by B_4C particulates that are located at grain boundaries.

Figure 6 shows the EDS analyses of pure Mg and MMCs. According to EDX analysis of pure Mg, point 1 belongs to Mg matrix and includes O (1.63 wt%) and Mg (98.37 wt%). Grain boundary (point 2) includes O (1.85 wt%) and Mg (1.85 wt%). The reason of low oxygen

Fig. 6 EDS analyses of pure Mg and MMCs

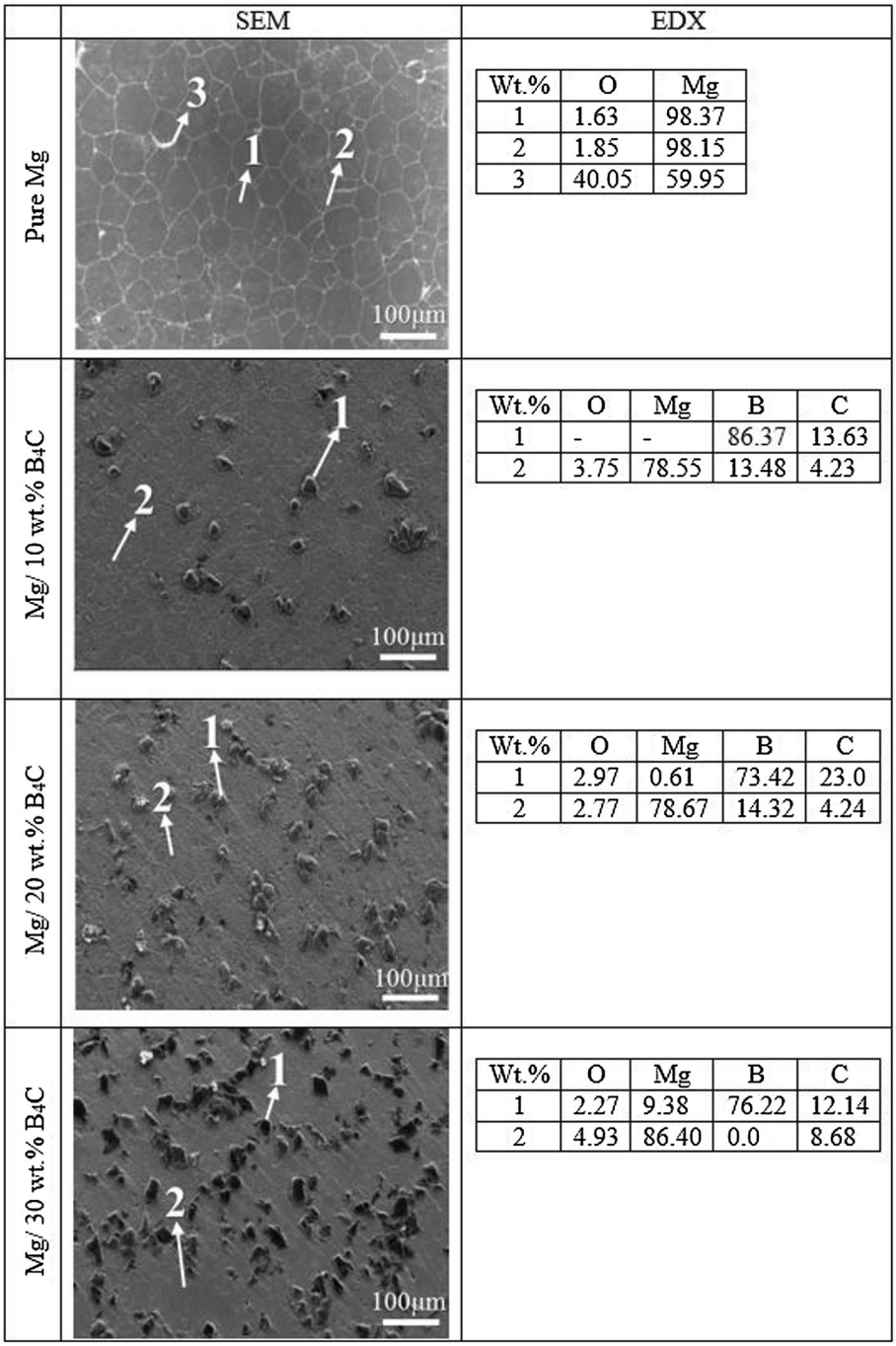

content is attributed to the production of samples under argon atmosphere. However, it is possible to say that MgO (point 3) is present due to high O (40.05 wt%) and Mg (59.95 wt%) content. Based on EDX analyses of MMCs, it is clearly seen that B_4C particulates (point 1) are present due to high B and C content in all composites. Generally, O content increases with increasing B_4C particulates. The reason of oxidation of B_4C particulates can be attributed to the fact that B_4C is prone to oxidation under oxygen-containing environment. Generally, a layer of B_2O_3 occurs on the surface of B_4C particulates [19].

Figure 7 shows the XRD patterns of the pure Mg and MMCs. From the XRD analyses, it can be seen that three main phases of Mg, B_4C and MgO are present in the structure. It can be said that the intensities of B_4C diffraction peaks are almost proportional to the amount of B_4C from 10 to 30 wt%. Additionally, intensity of Mg diffraction peaks decreases with increasing B_4C content.

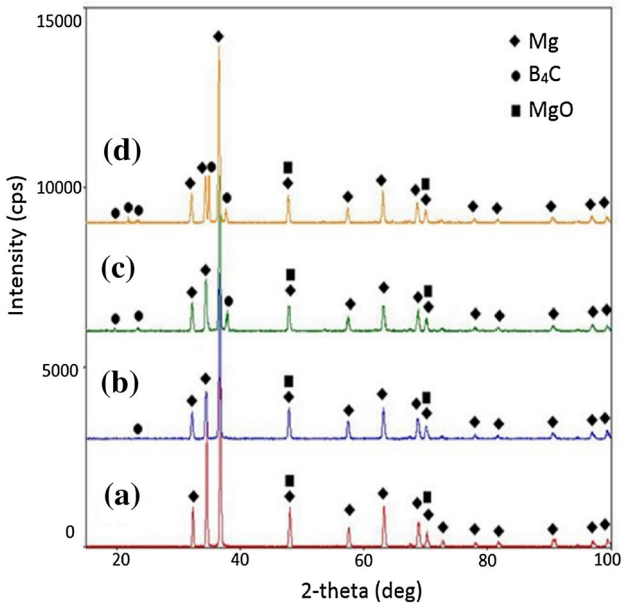

Fig. 7 XRD patterns of **a** pure Mg, **b** Mg/10 wt% B_4C, **c** Mg/20 wt% B_4C, **d** Mg/30 wt% B_4C

Also, phase of MgO is detected in all samples. The formation of MgO can be attributed to the high chemical activity between Mg and O during sintering process [27]. However, intensity of MgO is low due to the production of powders under argon atmosphere. Possible reactions for Mg/B_4C composites are given below [19];

$$2Mg + O_2 = 2MgO \quad (1)$$

$$Mg + 2B = MgB_2 \quad (2)$$

$$B_4C + 4O_2 = 2B_2O_3 + CO_2 \quad (3)$$

$$4Mg + B_2O_3 = 3MgO + MgB_2 \quad (4)$$

3.3 Hardness Results

Figure 8 shows the dependence of hardness on different particulate contents. Increments on hardness values of the MMCs are 29, 52.2 and 63.9%, respectively, for 10, 20 and 30 wt% B_4C. It is clear that hardness increases with increasing particulate content. The increase in hardness can be attributed to grain refinement and the presence of harder reinforcement in the matrix. Reinforcement particulates act as constraints to localized matrix deformation during indentation [26, 30].

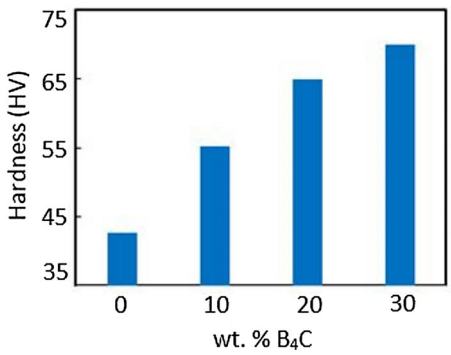

Fig. 8 Hardness values versus particulate percentages

Kevorkijan et al. [5] produced Mg-B_4C (50 vol%) composite via pressureless infiltration. They reported the hardness of 39 and 80 (HRC) for the pure Mg and Mg/50 vol% B_4C, respectively. Ghasali et al. [6] fabricated Mg/5 wt% B_4C composites by microwave and spark plasma sintering (SPS). The reported hardness values for microwave and SPS are 61 and 92 (HV), respectively. The higher hardness values obtained by SPS can be attributed to the pore-and microcrack-free microstructure. Jiang et al. [19] observed an increase in hardness with increasing particulate content for Mg-B_4C composites by powder metallurgy. They reported the hardness values as 44 and 133 (HB) for the 10 and 20 vol% B_4C respectively. Guleryuz et al. [31] manufactured pure Mg and Mg/B_4C (3, 6 and 9 wt%) composites by powder metallurgy. The reported hardness values for pure Mg and Mg/9 wt% B_4C are 38 and 55 (HB), respectively. The increase in hardness can be attributed to the homogenous distribution of hard B_4C particulates in soft Mg matrix.

Sıngh et al. [32] also fabricated Mg/B_4C (3, 6, 9 and 12 wt%) composites via stir casting. The hardness exhibited by Mg and Mg/12 wt% B_4C specimens are of 32 and 72 (HV), respectively. The increase in hardness may be mainly associated with harder B_4C particulates that prevent localized matrix deformation. Based on the literature, it can be concluded that the hardness values are increased with the addition of B_4C particulates. Hardness and hardness increment values obtained in this study are similar to the literature studies.

3.4 Compression Test Results

Table 5 shows the results of compression tests of pure Mg and MMCs. As seen in Table 5, 0.2% compressive yield strength (CYS) values increases with increasing B_4C content. As compared to pure Mg, increments on CYS values of the MMCs are 21.9, 49.7 and 69.5%, respectively, for 10, 20 and 30 wt% B_4C. Also, it can be seen that failure strain (FS) of materials decreases with the addition of B_4C. Figure 9 shows the compression test results as graphs.

There are some strengthening mechanisms which increase the CYS in metal matrix composites. These are;

1. Thermal and elastic modulus mismatch between the matrix and the reinforcement (due to high dislocation density)

Table 5 Compressive yield strength, ultimate compressive strength and failure strain % values of pure Mg and MMCs

Materials	0.2% CYS (MPa)	UCS (MPa)	Failure strain (FS) %
Pure Mg	83.06	222.52	18.46
Mg/10 wt% B_4C	101.29	196.08	14.38
Mg/20 wt% B_4C	124.35	204.73	12.67
Mg/30 wt% B_4C	140.82	204.44	9.74

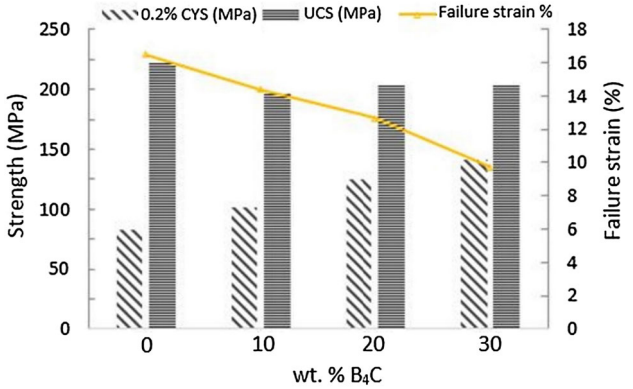

Fig. 9 Strength and failure strain values versus particulate percentages

Presence of reinforcements increases the CYS because they cause inhomogeneous deformation and high density dislocations. The increase in dislocation density in the composite material is related to mismatch of the elastic modulus (E) (E of Mg and B_4C are 41 and 472 GPa, respectively) and coefficient of thermal expansion (CTE) (CTE of Mg and B_4C are 28.9×10^{-6} and 5.0×10^{-6} K^{-1}, respectively) between the matrix and the reinforcement material [1, 16]. Therefore, this large difference in CTE and E values lead to the formation of dislocations and increase the strength [33].

2. Load bearing effects due to the presence of reinforcement

Load transfer depends on interfacial bonding between the matrix and the reinforcement [1]. Load transfer occurs from soft Mg matrix to hard inclusions (B_4C particulates). Interfacial bonding depends on volume rate of inclusion phases [25]. According to EDX and XRD analyses, phases of B_4C and MgO are detected as inclusions. It can be said that the reason of increase in CYS values in MMCs is the presence of these inclusions.

Lu et al. [34] manufactured Mg9%Al/Mg_2Si composite by powder metallurgy. The presence of MgO can be verified by XRD analysis. They reported that MgO acts as

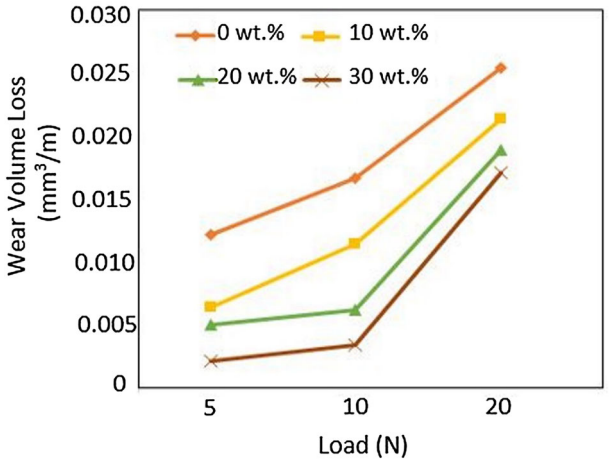

Fig. 10 Wear volume loss versus applied loads and particulate percentages

reinforcement which leads to increase in hardness and strength but deteriorate the ductility due to poor interfacial bonding and its brittle structure. Xi et al. [27] also reported that dispersed MgO particles have strengthening effect on mechanical properties in Ti–6Al–4V/Mg composites. In this study, it is possible to say that the presence of MgO contribute to increase CYS. However, it can be said that the effect of MgO on strength is little due to its low content (Fig. 6). The low UCS values of the composites can be attributed to the presence of the porosities and agglomeration of B_4C particulates. Hence, strengthening mechanism is not effective in these situations. Deng et al. [30] fabricated AZ91/SiC composites by stir casting. They reported that UTS decreases with agglomeration of SiC particulates.

3. Orowan strengthening

Orowan strengthening is an effective mechanism for nanocomposites [1, 25]. However, orowan strengthening is not possible because microparticulates have been used for this study.

4. Hall–Petch effect (grain size refinement)

The increase in CYS is related to the inverse proportion of strength with grain size according to Hall–Petch equation [1]. In this study, grain refinement is observed in MMCs (Fig. 4). Therefore, it is concluded that grain refinement plays an important role in increasing the CYS.

5. Ductility

Final fracture or capability of plastic deformation is related to crack initiation and progress in MMCs. Fracture can be attributed to: (a) mismatch between the reinforcement and the metallic matrix and (b) presence of voids. It is not possible to remove porosities completely in composites.

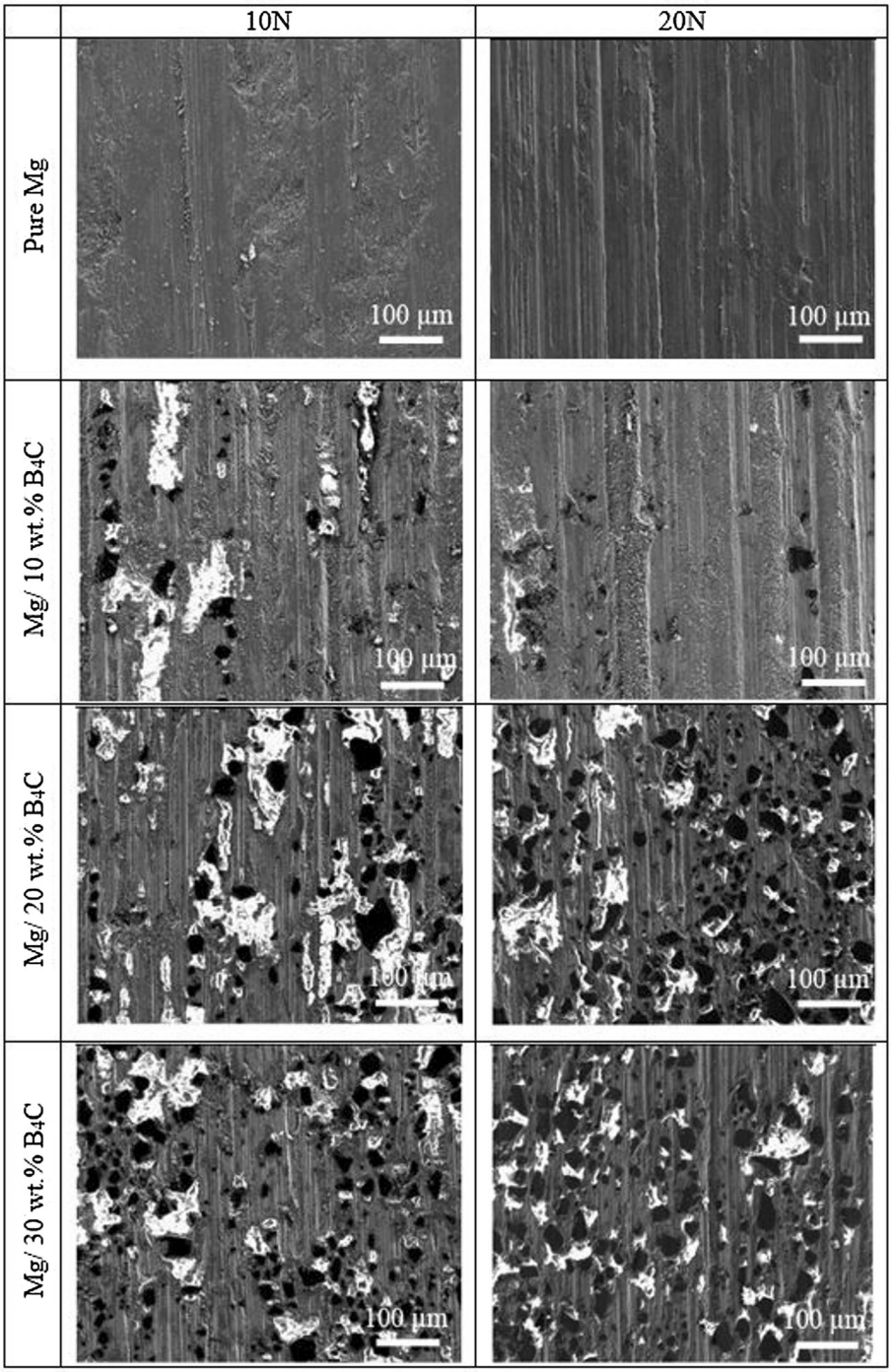

Fig. 11 Worn surface images of samples under loads of 10 and 20 N

Increase in porosity by the addition of reinforcements causes Mg/B_4C interface to be weak [25]. Values of UCS for composites can not be similar to that for pure Mg because the porosity values are higher than pure Mg. The reason of decrease in failure strain of MMCs is the presence of ceramic reinforcements which reduces ductility in composite materials. To increase the ductility, low porosity and uniform distribution of reinforcement are required [1].

3.5 Wear Results

Figure 10 shows the dependence of wear volume loss on different loads and particulate contents. As seen in Fig. 10, wear resistance significantly increases with increasing B_4C content. A sharp increase in wear volume loss is observed in the transition of load from 10 to 20 N. The wear volume loss is 0.012 for pure Mg, and 0.002 for Mg/30 wt% B_4C

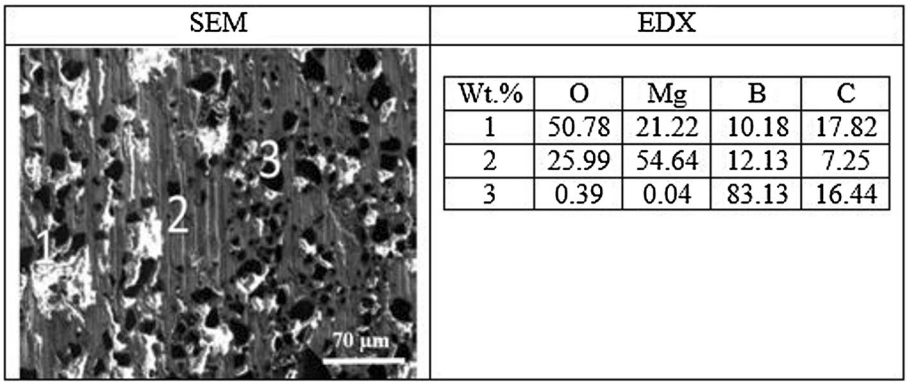

Fig. 12 EDX analysis of worn surface of Mg/20 wt% B_4C composite under load of 20 N

under load of 5 N. For load of 20 N, the wear volume loss of pure Mg and Mg/30 wt% B_4C are 0.025 and 0.017, respectively. The most important reason for the increase in wear resistance is the hard B_4C particulates which are stable during wear. The wear results are in agreement with Archard's law, which reports the inversely proportional relation between wear resistance of a material and its hardness [35].

Figure 11 shows the worn surfaces of pure Mg and MMCs under loads of 10 and 20 N. For pure Mg, it is concluded that wear mechanism is abrasive due to the presence of grooves for all loads. However, in the transition of load from 10 to 20 N, distinct grooves are present. As seen in Fig. 11, oxide areas (white) under load of 10 N are higher than load of 20 N. This is related to removing oxide layer by counter-face material under high load (20 N). Therefore, it is possible to say that wear mechanism is oxidation assisted abrasive for MMCs under load of 10 N. Under load of 20 N, MMCs exhibit partly oxidative and severe abrasive wear behaviour. Pure Mg exhibits severe wear, but Mg/30 wt% B_4C shows the least wear.

Figure 12 shows the EDX analysis of worn surface of Mg/20 wt% B_4C under load of 20 N. It can be said that MgO is present due to high Mg and O content after wear test. It is also concluded that B_4C particulates are present because of high B and C content. Additionally, it is observed that B_4C particulates break during wear.

4 Conclusion

In summary, pure Mg and 10, 20 and 30 wt% B_4C reinforced MMCs were successfully produced by powder metallurgy using hot pressing. The porosities of the samples increased with an increase in B_4C content. Distribution of homogenous particulates and grain refinements were observed in MMCs. The addition of B_4C particulates led to significant increase in CYS. A significant increase in hardness and wear resistance was achieved by increasing B_4C content. For all wear loads, Mg/30 wt% B_4C composite had the highest wear resistance. Abrasive and oxidative wear mechanisms were observed. B_4C particulates, which were stable during wear, were the most important reason for increasing wear resistance. As a result, Mg/B_4C composites that were produced by powder metallurgy were possible materials for applications which required wear resistance.

Acknowledgements This work was supported by Karabuk University Coordinatorship of Research Projects (Project Number: KBU-BAP No.16/1-DR-077).

References

1. Gupta M, and Sharon N M L, *Magnes Magnesium alloys and Magnesium Composites*, John Wiley & Sons Inc. Publication, New Jersey (2011), p 103.
2. Dey A, and Pandey K M, *Rev Adv Mater Sci* **42** (2015) 58.
3. Mahajan G V, and Aher V S, *Int. J Sci Res Publ* **2** (2012) 11.
4. Lee K B, Kım Y S, and Kwon H, *Metall Mater Trans A* **29** (1998) 3087.
5. Kevorkijan V, and Škapin S D, *Mater Manuf Processes* **24** (2009) 1337.
6. Ghasali E, Alizadeh M, Niazmand M, and Ebadzadeh T, *J Alloys Compd* **697** (2017) 200.
7. Ye H Z, and Lıu X Y, *J Mater Sci* **39** (2004) 6153.
8. Wang H Y, Jiang Q C, Wang Y, Ma B X, and Zhao F, *Mater Lett* **58** (2004) 3509.
9. Chua B W, Lu L, and Lai M O, *Compos Struct* **47** (1999) 595.
10. Garces G, Perez P, and Adeva P *Scripta Mater* **52** (2005) 615.
11. Ferkel H, and Mordike B L, *Mater Sci Eng A* **298** (2001) 193.
12. Hassan S F, and Gupta M, *Metall Mater Trans A* **36** (2005) 2253.
13. Wong W L E, Karthik S, and Gupta M, *Mater Sci Technol* **21** (2005) 1063.
14. Contreras A, Lopez V H, and Bedolla E, *Scripta Mater* **51** (2004) 249.
15. Li Q, and Tian B, *J Mater Res* **28** (2013) 1877.
16. Domnich V, Reynaud S, Haber R A, and Chhowalla M, *J Am Ceram Soc* **94** (2011) 3605.
17. Kevorkijan V, and Škapin S D, *MJoM* **15** (2009) 3.
18. Yao Y, and Chen L, *J Mater Sci Technol* **30** (2014) 661.
19. Jiang Q C, Wang H Y, Ma B X, Wang Y, and Zhao F, *J Alloys Compd* **386** (2005) 177.

20. Spierings A B, Schneider M, and Eggenberger R, *Rapid Prototyp J* **17** (2011) 380.
21. Feeman T G, *Int J Math Edu Sci Technol* **40** (2009) 1118.
22. Yar A A, Montazerian M, Abdizadeh H, and Baharvandi H R, *J Alloys Compd* **484** (2009) 400.
23. Nguyen Q B, Quader I, Nai, M L S, Seetharaman S, Leong E W W, Almajid A, and Gupta M, *Powder Metall* **59** (2016) 209.
24. Narayanasamy P and Selvakuma R N, *Trans Nonferrous Met Soc China* **27** (2017) 312.
25. Thakur S K, Srivatsan T S, and Gupta M, *Mater Sci Eng A* **466** (2007) 32.
26. Rashad M, Pan F, Tang A, Asif M, and Aamir M, *J Alloys Compd* **603** (2014) 111.
27. Xi Y L, Chai D L, Zhang W X, and Zhou J E, *Mater Lett* **59** (2005) 1831.
28. Liu J, Zhao K, Zhang M, Wang Y, and An L, *Mater Lett* **143** (2015) 287.
29. Bagchesara M A, and Abdizadeh H, *J Mech Sci Technol* **26** (2012) 367.
30. Deng K K, Wu K, Wu Y W, Nie K B, and Zheng M Y, *J Alloys Compd* **504** (2010) 542.
31. Guleryuz L F, Ozan S, Uzunsoy D, and Ipek R, *Powder Metall Met Ceram* **51** (2012) 456.
32. Sıngh A, and Bala N, *Metall Mater Trans A*, **48** (2017) 5031.
33. Habibi M K, Hamouda A S, and Gupta M, *J Alloys Compd* **550** (2013) 83.
34. Lu L, Thong K K, and Gupta M, *Compos Sci Technol* **63** (2003) 627.
35. Muley S V, Singh S P, Sinha P, Bhingole P P, and Chaudhari G P, *Mater Des* **53** (2014) 475.